

RAMAN SPECTROSCOPY STUDIES OF SOME CARBON MOLECULAR SIEVES

C. SISU^{a*}, R. IORDANESCU^b, V. STANCIU^a, I. STEFANESCU^a,
A. M. VLAICU^c, V. V. GRECU^d

^aNational R&D Institute for Cryogenics and Isotopic Technologies, Rm. Valcea,

^bNational R&D Institute for Optoelectronics – INOE 2000, Bucharest,

^cNational R&D Institute for Materials Physics, Bucharest,

^dUniversity of Bucharest, Faculty of Physics, Bucharest.

Structural characterization by Raman spectroscopy and XRD of some carbon molecular sieves is described. These materials, prepared by standard procedure from a native pitcoal, have a turbostratic structure consisting of nanodimensional graphitic platelets, disorderly oriented in a hard amorphous network. In plane dimension of these platelets is obtained from Raman spectra according to Tuinstra-Koenig relation relating this dimension to the ratio of the graphitic and disorder bands intensities, $I(D)/I(G)$. XRD spectra, characteristic to amorphous carbons, allow determination of the platelet widths using Scherrer's relation. Both methods give information only about the crystalline part of the material. The data for precursor material and two molecular sieves, used for O_2/N_2 , respectively CO_2/CH_4 separation, are presented. The similarity of the results for all samples demonstrate that the preparation procedures of molecular sieves from the precursor, impregnation with a polymer material followed by a reheat in nitrogen atmosphere at about $800^{\circ}C$, does not change essentially the crystalline part of the materials.

(Received February 25, 2016; Accepted April 22, 2016)

Keywords: Carbon molecular sieves, Raman spectra XRD diffraction data,
Dimensions of graphitic platelets

1. Introduction

Carbon molecular sieves, CMS, as well as other forms of activated carbons, are selective adsorbents with important applications in chemical and petrochemical industries, in separation and catalytic processes [1, 2]. They are very efficient in separation and purification of gases having similar molecular dimensions. In particular they are used in two commercially important separations, O_2/N_2 and CO_2/CH_4 . The first process is largely used for production of pure oxygen and nitrogen from air by pressure swing adsorption, PSA, [3-5]. The second process is important for purification of natural gases [5]. Other important applications are in CO_2 adsorption for air depollution [6], gas storage applications, in separation of bio-components from solutions [7], or depollution of waste liquids/water.

There are several methods to produce carbon molecular sieves, CMS [8-11]. In general it starts with selection of an appropriate precursor, a carbonic non-graphitizing material. Such a material is highly porous, with a wide range of pore size distribution. It is necessary to reduce these sizes to the range of molecular diameters of gases which are going to be separated, together with narrowing the size distribution domain. A very efficient way to achieve this is to impregnate the precursor with a hydrocarbon or polymer material followed by an appropriate high temperature pyrolysis [9]. The efficiency of the obtained material depends on precursor nature and structure as well on the choice of polymer membrane and pyrolysis process.

*Corresponding author: claudia_sisu@yahoo.co.uk

A large variety of methods are used for characterization of both the precursor and final CMS material. Stationary and non-stationary adsorption studies give information about pore size distribution and the adsorption kinetics [12-14]. In the same time structural characterization proved to be important for explaining the selectivity differences. X-ray diffraction and spectroscopic methods (FTIR and Raman spectroscopy in particular) have been used over decades to elucidate the internal structure, porosity degree and specific activity of these materials. In this paper Raman spectroscopy and XRD have been used to characterize a coal precursor and the molecular sieves derived from it by the standard procedure.

2. Experimental results and discussion.

The carbon precursor for the preparation of CMS support was a pitcoal sample from Petrila mine, Hunedoara country, Romania. The flow chart for preparation technology was described in [23]. A brief description is the following: oxidized coal powder (crushed pitcoal sample was oxidized in air at 250⁰C for 4-5 hours) was mixed with a solution of pitch and starch dissolved in benzene. Extruded pellets were carbonized at 650-750⁰C in a N₂ flow for 30 min. The reactor heating rate was 5 degrees per minute; cooling was performed also in N₂ atmosphere. The obtained material, the CMS support, had a large pore size distribution and low separation selectivity. To narrow the pore sizes to the required molecular dimensions carbon deposition inside the pores was made by impregnating the support with a solution of polystyrene (2-4 wt%) in benzene, and then pyrolyzed at 750-800⁰C in N₂ flow. The product, carbon molecular sieves membrane, CMSMs, was removed at room temperature. Sample notations are: pitcoal, P1-CMS support (precursor), P2-CMSMs(O₂/N₂), P3-CMSMs(CO₂/CH₄)

XRD has been used to characterize and explain coal and carbonaceous materials for a long time. The first studies date back to B. E. Warren and R. E. Franklin researches [15, 16]. Actually R. Franklin has introduced the concept of non-graphitizable carbons, namely, carbon materials which do not graphitize even at very high temperature. Their structure consists of nanosized graphite platelets, having disordered orientations in space, inter-bonded by strong amorphous carbon regions (the turbostratic structure). This model is even now accepted, also it is very approximate as it does not precise the nature of the amorphous bonding domains. Their work has been continued by many researcher groups [17-19], by using elaborated mathematical procedures for the analysis of the diffraction diagrams. Recent studies, with high resolution electron microscopy, have shown that in the amorphous network regions fullerene-like bonds between carbon atoms occur [20]. In the diffraction diagrams broad peaks are observed. Only (00l) peaks – due to inter-layer scattering and (hk0) peaks – due to intra-layer scattering peaks are observable [16,21]. No maxima of (hkl) type with $l \neq 0$ are observed consequence of disordered orientations of graphitic nano-platelets. From their positions inter-layer distances between graphitic planes are determined, and from the peak widths crystallite sizes can be evaluated using the conventional Scherrer equations [21,22].

The XRD measurements were performed on a Bruker-AXS D8-Advanced System, using the Bragg-Brentano setup, with copper X-ray generator and a one-dimensional array detector. The 2 θ sweep range was 10⁰-100⁰, step-width 0.05⁰ and counting time 2 sec. Specific XRD diagrams are given in Fig.1; the de-convolution of the pitcole XRD spectrum is given on the bottom of the figure.

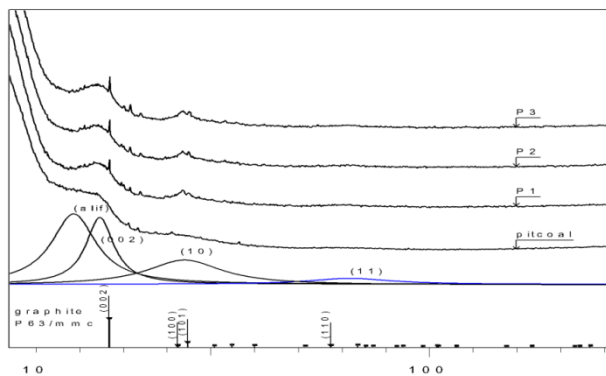


Fig.1 XRD spectra of pitcoal and P1, P2, P3 samples

The diffraction spectra were decomposed into a series of peaks; the background caused by the sample amorphous phase and air scattering together with an additional linear background was fitted with a fourth order polynomial in $1/2\theta$ toward small diffraction angles. There are 4 broad peaks associated to the main turbostratic phase in the following 2θ ranges, 24° - 25° - the diffraction on (002) plane, 44° - 48° - (10) plane, 80° - 82° - (11) plane, and 18° - 20° the so-called γ peak. This last band is attributed to saturated carbons by aliphatic chains on the edges of graphene nanoplatelets [21,24]. The very sharp peaks do not belong to turbostratic carbon material. They might be due to mineral impurities in the pit coal sample, but no successful identification was obtained; as even after a HCL+HF demineralization these peaks did not disappear crystalline carbon phases might exist in the samples; their concentration is small, only tens of percent, and does not change significantly between the samples. We consider that they do not influence the material structure and properties.

The following parameters were determined. Peak positions gave interlayer distances, $d_{hkl} = n(\lambda/2\sin\theta_{hkl})$ and their half widths allow the calculation of nano-platelet dimensions using Scherrer's formula, $L_j = K_j(\lambda/\Delta_j \cos\theta_j)$, K_j being Scherrer constant. Thus the interlayer distance is determined from (002) peak position, $d_{002} = \lambda/2\sin\theta_{002}$, the c-axis correlation length is $L_c = 0.89(\lambda/\Delta_{002} \cos\theta_{002})$, and in plane correlation length is obtained from $L_a = 1.84(\lambda/\Delta_{hk} \cos\theta_{hk})$; for coals and CMSs (hk) peaks are usually (10) and (11) peaks. An aromaticity factor can be defined as:

$$f_a = C_{ar}/(C_{ar} + C_{al}) = I_{002}/(I_{002} + I_\gamma),$$

where C_{ar} and C_{al} are the numbers of aromatic and respectively aliphatic carbons, proportional to (002) and γ bands intensities, I_{002} and I_γ .

In table 1 values for pitcoal and P1-P3 samples are summarized:

Table 1 Structural data for investigated samples

Sample	Sample nature	$d_{002}(\text{nm})$ (± 0.002)	$L_c(\text{nm})$ (± 0.02)	Aromaticity f_a	$L_a(\text{nm})$ (± 0.05)
Pitcoal	Pitcoal	0.364	1.18	0.51	1.02
P ₁	CMS precursor	0.363	1.08	0.79	3.68
P ₂	CMSMs(O ₂)	0.366	0.99	0.86	2.86
P ₃	CMSMs(CO ₂)	0.370	0.99	0.88	3.68

We have to notice that these values are mean values, therefore the increase of graphene platelets dimensions after the heat treatment for CMS precursor preparation must be interpreted more as an effect of small, volatile platelets elimination than a systematic increase of their dimensions. This interpretation is supported also by the significant increase of f_a factor. The values for in plane dimension, L_a , must be considered carefully, as they were determined from the width of (10) peak, which is rather small and the errors due to diffraction spectrum processing can be

significant. As expected the distance d_{002} of graphitic nanoplatelets is larger than in bulk graphite, and the number of stacked graphitic planes is small, 4-5 planes. Concerning the crystalline sizes in the graphitic planes they are larger compared with bulk graphite; this can be seen from the larger 2θ values of (10) and (11) diffraction peaks than in graphite.

Raman spectroscopy has been and it is largely used in characterizing the solid materials in general and carbon materials in special [25]; its usefulness comes from the fact that the vibration spectra of solid compounds are much simpler than the IR spectra and are characteristic to complexes existing in the material. The two spectroscopic methods are complementary, as their selection rules are different. In graphite there are 6 normal vibration modes at $q=0$ which can be determined by group theory methods [26],

$$\Gamma_{\text{vib,2D}} = A_{2g} + B_{2g} + E_{1u} + E_{2g},$$

E_{2g} stretching mode being the only one Raman active. The corresponding Raman transitions occur in graphite at 1583 cm^{-1} , and it is known as G-band. Even graphite crystals present an in plane disorder manifesting in Raman spectra by another band around $1340\text{-}1360 \text{ cm}^{-1}$, the so called D-band (disorder band) [25-28]. Their positions and widths depend on the material carbonization degree and also on the disorder (porosity, crystallite size distribution, concentration of amorphous component). In consequence Raman spectra give information on all such questions. The origin of D-band is attributed to double resonant Raman process close to K point of the graphite Brillouin zone [26, 27]. Its intensity scales with the size of micro crystals, i.e. with the degree of long range order of the lattice [28-30]. It is also dispersive, its position depending on the excitation radiation wavelength [32]. This shift is strong, $\sim 50 \text{ cm}^{-1}/\text{eV}$ [33]. Second order spectra are also observed, D^* - band (called also G^* -band) having almost double frequency of D-band, G^* - band the second order overtone of G-band. An important result, according to Tuinstra and Koenig, relates the ratio of G and D band to in plane crystallite sizes (in plane coherence length),

$$I(D)/I(G) = C(\lambda)(1/L_a),$$

$C(515.5\text{nm}) = 4,4\text{nm}$; this correlation is valid for crystallites $L_a > 2\text{nm}$ [30].

The Raman spectra have been carried out on a Jobin-Yvonne LabRam Spectrometer at three excitation wavelengths, 488, 514, 633 nm. Laser power on the sample was 10.23 mW, exposing time 5 sec; each spectrum was 5 times accumulated. In figure 2 characteristic spectra are given.

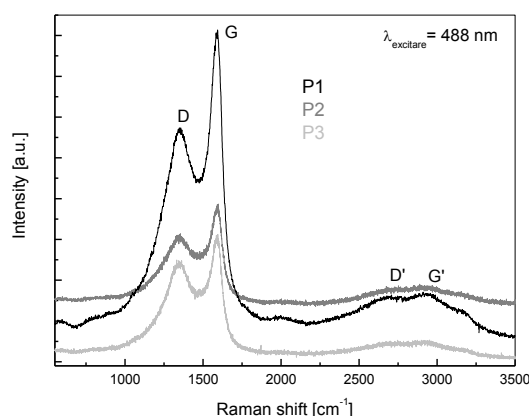


Fig.2 Raman spectra, excitation wavelength 488 nm

Raman spectra appear in two frequency domains, $1340\text{-}1650 \text{ cm}^{-1}$, corresponding to G and D bands characteristic to carbon compounds, and $2600\text{-}3400$, corresponding to G and D bands overtones and the D-G inter-combination band; transitions corresponding to more complex crystalline networks like in carbonic fibers are as well possible [34]. The spectra have been de-

convoluted in Lorentz components; an example is given in Fig. 3a,b (sample 1, excitation wavelength 488 nm.).

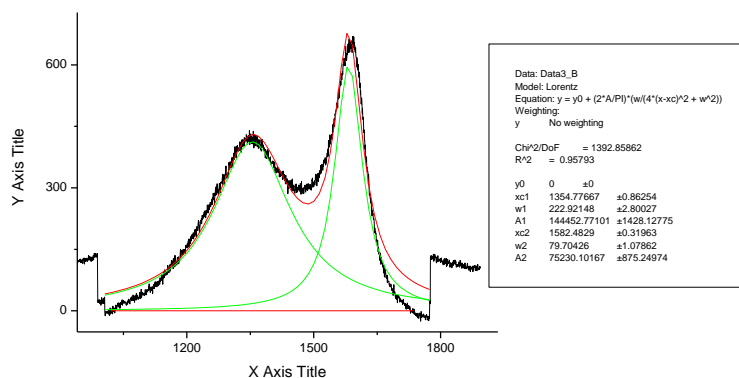


Fig.3a. Sample P1, G and D bands de-convolution, $\lambda_{exc}=488$ nm

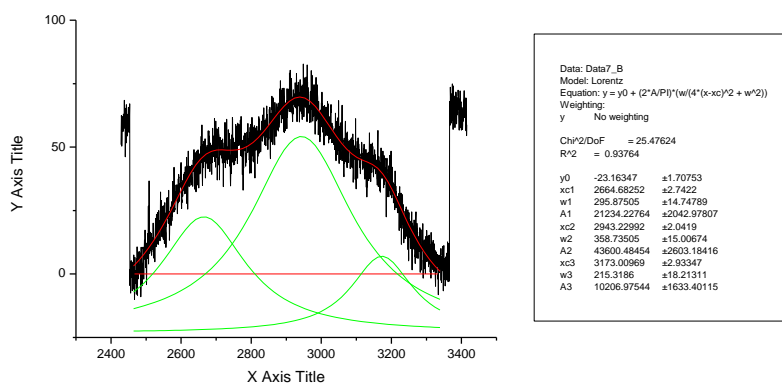


Fig. 3b. Sample P1, deconvolution in spectral range 2500-3300 cm^{-1} , three bands are put in evidence (overtone of D and G bands and the intercombination band)

Similar simulations have been performed for all spectra with an acceptable χ^2 factor. In the 1200-1700 spectral domain no other bands exist, allowing the determination of the ratio $I(D)/I(G)$; results for these principal bands are summarized in table 2, and figure 4 and 5.

Table 2 Values of the main Raman bands for three excitation frequencies

Sample	$\lambda=488$ nm		$\lambda=514$ nm		$\lambda=633$ nm	
	D peak [cm^{-1}]	G peak [cm^{-1}]	D peak [cm^{-1}]	G peak [cm^{-1}]	D peak [cm^{-1}]	G peak [cm^{-1}]
P1	1354	1582	1348	1579	1337	1580
P2	1352	1584	1341	1590	1334	1581
P3	1351	1582	1346	1578	1336	1583

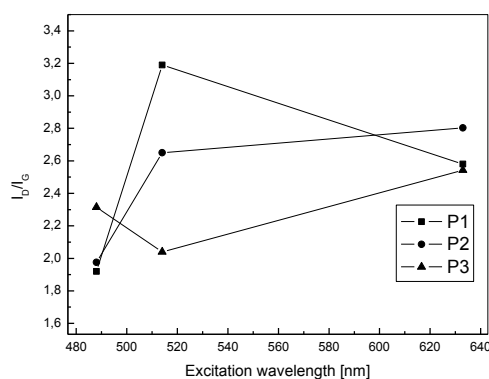


Fig. 4. The dependence of $I(D)/I(G)$ ratio on excitation wavelength

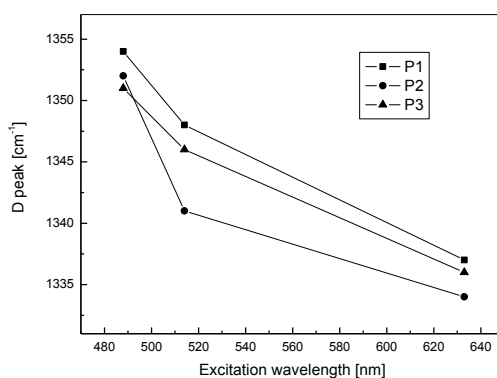


Fig. 5. D peak position dependence on excitation wavelength

These data show a quasi independence on excitation frequency of the G band position, in accordance with literature (the mean values are given in table 3). D band position is evidently dispersive, its value increases with excitation frequency. Concerning the dependence of $I(D)/I(G)$ ratio contradictory results are obtained. According to Mathews and col. [35] $C(\lambda) = C_0 + C_1 \lambda$, where $C_0 = -12.6$ nm, $C_1 = 0.033$. Therefore the ratio must increase for longer wavelengths. Our experimental data cannot be correlated with this linear dependence, but, except for the sample P1, an increase is put in evidence. Accepting the validity of Tuinstra-Koenig relation the in plane correlation length can be calculated. Using the data for 514 nm excitation the values given in table 3 are obtained.

Table 3 Calculated values of nano-crystallites in plane correlation length (excitation length 514nm)

Sample	$I(D)/I(G)$ (± 0.4)	L_a (nm) (± 0.4)	G peak (mean value)
Precursor, P1	3.20	1.37	1580 ± 3
CMSMs(O ₂), P2	2.64	1.66	1585 ± 4
CMSMs(CO ₂), P3	2.22	1.98	1581 ± 3

Comparing these values with those from XRD a rather large discrepancy is observed. It not surprising taking into account the possible errors in interpretation of XRD data and the limited validity of Tuinstra-Koenig relation at such small dimensions of crystallites. Both methods give an important qualitative information, namely that the studied CMS have similar low crystalline phase, with very small graphite like platelets randomly dispersed in an amorphous rigid matrix.

3. Conclusions

The structural investigation of precursor material and CMSMs obtained by impregnation-pyrolysis technique demonstrate their turbostratic structure, namely small crystalline graphitic platelets randomly dispersed in a rigid amorphous network. The dimensions of graphitic crystalline platelets are of nm values. It is worth mentioning that both methods refer to bulk crystalline phase. They give no information about surface bonds like C-O, C-H, etc., other methods like IR spectroscopy being necessary. A significant fact is that compared with the CMS precursor both CMSMs obtained through the mentioned technology have comparable crystalline structural characteristics. Thus the carbonic material deposited on the inner pore walls does not change significantly the turbostratic structure of the precursor crystalline phase. For such a complex system this conclusion is significant.

Acknowledgements

The authors are indebted to Mr. Ionut Fieraru for Raman measurements.

References

- [1] H. Marsh, F. Rodriguez-Reinoso, Activated Carbon, Elsevier Ltd., Oxford, 2006.
- [2] J. N. Armor, Separation Technology, Elsevier Science Publ., Amsterdam, 1994.
- [3] D. M. Ruthven, S. Farooq, K. S. Knaebel, Pressure Swing Adsorption, VCH-Wiley, 1993.
- [4] C. A. Grande, Int. Scholarly Res. Notions – Chem. Eng., **vol. 2012** (2012), ID article 982934, 12 pages.
- [5] C. R. Reid, K. M. Thomas, Langmuir, **15**, 3206 (1999).
- [6] A. Wahby, J. M. Ramos-Fernandez, M. Martinez-Escandell, A. Sepelveda-Escribano, J. Silvestre-Albero, F. Rodriguez-Reinoso, Chem. Sus, Chem, **23**, 974 (2010).
- [7] A. Vinu, M. Miyahara, K. Areqa, J. Nanosci. Nanotechn., **6**, 1510 (2006).
- [8] V. C. Stanciu, The separation of gases through selective diffusion (in roumanian), PhD Thesis, Univ. Babes-Bolyai, Cluj-Napoca, 1997.
- [9] S. M. Saufi, A. F. Ismail, Carbon, **42**, 241 (2004).
- [10] H. C. Foley, Macroporous Materials, **4**, 407 (1995)
- [11] R. F. P. M. Moreira, H. J. Jose, A. E. Rodrigues, Carbon, **39**, 2269 (2001).
- [12] L. F. Herrera, C. Fan, D. D. Do, D. Nicholson, Ind. Eng. Chem. Res., **50**, 4150 (2011).
- [13] S. W. Rutherford, J. E. Coons, J. of Colloid & Interface Science, **284**, 432 (2005).
- [14] P. O'koye, M. Benham, K. M. Thomas, Langmuir, **13**, 4054 (1997).
- [15] E. B. Warren, Phys. Rev. **59**, 693 (1941).
- [16] R. E. Franklin, Acta Crystallografica, **3**, 107 (1950).
- [17] S. Ergun, V. H. Tiensuu, Fuel, **38**, 64 (1959).
- [18] D. L. Wertz, M. Bissell, Energy Fuel, **8**, 613 (1994).
- [19] H. Fujimoto, Carbon, **41**, 1585 (2003).
- [20] P. J. F. Harris, Critical Reviews in Solid State and Materials Sciences, **30** 235 (2005).
- [21] L. Lu, V. Sahajwalla, C. Kong, D. Harris, Carbon, **39**, 1821 (2001).
- [22] C. Weidenthaler, Nanoscale, **3**, 792 (2011).
- [23] V. Stanciu, D. Stefanescu, E. David, in Advances in Materials and Processing Technologies, A. M. S. Hamouda (ed), **1**, 72 (1998)
- [24] T. F. Yen, J. G. Erdman, S. S. Pollack, Anal. Chem., **33**, 1587 (1961).
- [25] J. R. Dennison, M. Holtz, G. Swain, Spectroscopy, **11**, 38 (1996).
- [26] S. Reich, C. Thomsen, Phil. Trans. Royal Soc. London, **A362**, 2271.
- [27] A. C. Ferrari, J. Robertson, Phys. Rev., **B61**, 14095, Phys. Rev., **B64**, 75414 (2001).
- [28] F. Tuinstra, J. L. Koenig, J. Chem. Phys., **53**, 1126 (1970).
- [29] L. G. Cancado, K. Takai, T. Enoki, M. Endo, Y. A. Kim, H. Mizusaki, N. L. Speziale,

- A. Jorrio, M. A. Pimenta, *Carbon*, **46**, 272 (2008).
- [30] G. A. Zigler, B. Smarsly, N. Gierlinger, H. Peterlik, O. Paris, *Carbon*, **44**, 3239 (2006).
- [31] P. Mallet-Ladeira, P. Puech, C. Toulouse, M. Cazayous, N. Ratel-Ramond, P. Weisbecker, L. G. Vignoles, M. Monthieux, *Carbon*, **80**, 629 (2014).
- [32] R. P. Vidano, D. B. Foschbach, L. J. Willis, T. M. Loehr, *Solid State Commun.* **39**, 341, (1981).
- [33] Y. Wang, D. C. Alsmeyer, R. L. McCreery, *Chem. Mater.*, **2**, 557 (1990).
- [34] T. Orfanoudaki, G. Skodras, I. Dolios, G. P. Sakellariopoulos, *Fuel*, **82**, 2045 (2003)
- [35] M. J. Mathews, M. A. Pimenta, G. Dresselhaus, M. S. Dresselhaus, M. Endo, *Phys. Rev.*, **B59**, R6585 (1999).